

An adaptive nonlinear elimination preconditioned inexact Newton algorithm for highly local nonlinear multicomponent PDE systems

Haijian Yang^a, Feng-Nan Hwang^{b,*}

^a*College of Mathematics and Econometrics, Hunan University, Changsha, Hunan, 410082, P. R. China*

^b*Department of Mathematics, National Central University, Zhongli District, Taoyuan City 32001, Taiwan*

Abstract

This work aims to develop an adaptive nonlinear elimination preconditioned inexact Newton method as the numerical solution of large sparse multi-component partial differential equation systems with highly local nonlinearity. A nonlinear elimination algorithm used as a nonlinear preconditioner has been shown to be a practical technique for enhancing the robustness and improving the efficiency of an inexact Newton method for some challenging problems, such as the transonic full potential problems. The basic idea of our method is to remove some components causing troubles in order to decrease the impact of local nonlinearity on the global system. The two key elements of the method are the valid identification of the to-be-eliminated components and the choice of subspace correction systems, respectively. In the method, we employ the point-wise residual component of nonlinear systems as an indicator for selecting these to-be-eliminated components adaptively and build a subspace nonlinear system consisting of the components corresponding to the bad region and an auxiliary linearized subsystem to reduce the interfacial jump pollution. The numerical results demonstrate that the new approach significantly improves performance for incompressible fluid flow and heat transfer problems with highly local nonlinearity when compared to the classical inexact Newton method.

Keywords: Fluid flow, Heat transfer, Adaptive nonlinear elimination, Highly local nonlinearity, Inexact Newton method

1. Introduction

A class of nonlinear preconditioned iterative algorithms, namely the additive Schwarz preconditioned inexact Newton algorithm (ASPIN) proposed by Cai and Keyes [4], opened up a new research direction on the development of nonlinear iterative solvers. In the past, the typical application of a preconditioner for nonlinear problems was usually employed together with a Krylov subspace method for the numerical solution of the Jacobian systems, e.g., the Newton-Krylov-Schwarz algorithm (NKS) [3, 21] and the Newton-Krylov-multigrid algorithm [22, 27], or for other similar linearized systems arisen from the Picard-type iterative method. The major role of linear preconditioners is to accelerate the convergence of an iterative method to obtain a high-quality Newton search direction, but it usually has nothing to do with helping to improve the robustness of an inexact Newton method if no good initial guess is available. On the other hand, ASPIN constructs the nonlinear preconditioner based on the overlapping Schwarz framework and applies it directly to the nonlinear system. In this case, the convergence of an inexact Newton method is not sensitive to the selection of an initial guess, physical parameters, e.g., the Reynolds number for the incompressible flows and the Mach number for the compressible flows, and the system parameters, e.g., geometric configuration, mesh sizes, etc. The basic idea of ASPIN is to reformulate the original nonlinear system as some easier-to-solve preconditioned nonlinear system implicitly and then solve the new

*Corresponding author.

Email addresses: haijianyang@hnu.edu.cn (Haijian Yang), hwangf@math.ncu.edu.tw (Feng-Nan Hwang)

system through an inexact Newton method. After more than ten years of progress, Cai and Keyes' work now draws much attention from the scientific community. Among them, ASPIN and its variants such as the multiplicative Schwarz version [24, 25, 26] or the restricted additive Schwarz version [12] have been applied successfully to incompressible high-Reynolds number flows [4, 5, 7, 17, 18], high-Rayleigh number convection flows [26], transonic compressible flows [6, 19, 38], multiphase flows in porous media [30, 32], unconstrained optimization problems arising in nonlinear elasticity problems [16], and image processing [39]. However, the nonlinear additive Schwarz preconditioner in the ASPIN belongs to the class of the *left* nonlinear preconditioners, which has some drawbacks. For example, the computational cost for the numerical evaluation of the nonlinear preconditioned function can be very expensive, since it requires to solve several subdomain nonlinear problems, although it can easily be parallelized due to the independence of these subdomain problems. The overhead of ASPIN can be more significant compared to the NKS algorithm, especially when the certain global Newton iteration requires to perform few backtracking steps, a commonly-used globalization technique to assure sufficient progress of Newton iteration. Hence, ASPIN is intended for the cases where classical Newton-type method fails to converge.

On the other hand, nonlinear preconditioning can be applied to the right of the nonlinear function. Instead of changing the function of the system itself as a left nonlinear preconditioner does, right preconditioning modifies the unknown variables of the nonlinear system. Also, right nonlinear preconditioning can be interpreted as nonlinear coordinate transformation between the solution spaces, see Ref. [35], where Yang et al. used a simple example to illustrate this idea. Hwang et al. [19, 20] employed a nonlinear elimination (NE) technique [23] as a right preconditioner for the 1D and 2D transonic full potential flow problems. The basic idea of NE is to remove these components that cause trouble for IN implicitly. An effective identification of the to-be-eliminated variable set is the critical step for the success of the overall algorithm. One possible strategy to determine which components to eliminate based on a priori knowledge or feedback from the intermediate numerical solution. For example, the numerical local Mach number provides such useful information, where the shock wave is located, which corresponds to the highly local nonlinear components to be eliminated in the transonic flow calculations [20].

The objectives of this work are to develop a class of adaptive NE preconditioners for the multicomponent systems with highly local nonlinearities and to study numerically the robustness and efficiency of the IN method preconditioned by NE for some challenging flow problems, including high-Reynolds number forced and mixed convection cavity flow problems. In general, designing effective elimination strategies for multicomponent systems is not trivial, since each variable interacts with the others. One possible elimination strategy is based on the field variable. For example, Lanzkron et al. [23] considered the drift-diffusion equations consisting of the Poisson equation and both the electron and hole continuity equations for the semiconductor device simulation. Their numerical result showed that when the field variables corresponding to the two continuity equations are selected to eliminate, the efficiency of the classical IN is significantly improved by using together with the nonlinear elimination technique. Further successful application examples of the field variable based NEs were the thermal convective flow control problem [35] and the two-phase porous media flow problem [37]. On the other hand, we adopt the domain decomposition elimination approach, i.e., when one variable on some particular mesh point is selected to eliminate, all other variables corresponding to that mesh point are also eliminated. In this work, we perform some numerical experiments to obtain some insight about how to design the elimination process and study several different elimination strategies.

The remainder of the paper is structured as follows. In Section 2, we give a general description of the *right* nonlinear elimination preconditioned inexact Newton algorithm for PDE problems with highly local nonlinearity. In Section 3, we introduce the governing equations for fluid flows and heat transfer, which are our target applications, together with their discretizations. In Section 4, we introduce the nonlinear elimination preconditioner for the multicomponent PDEs. In Section 5, we present some numerical results for two benchmark problems, including lid-driven cavity flow problem and forced convective heat transfer problem. We conclude this paper in Section 6.

2. A framework of right NE preconditioned inexact Newton algorithm

We consider an inexact Newton method with backtracking technique (INB) [11, 13] in conjunction with a right nonlinear elimination preconditioner for finding a root of the large, sparse, nonlinear system of equations,

$$F(x) = 0, \quad (1)$$

where $F : \mathbb{R}^n \rightarrow \mathbb{R}^n$ is a given nonlinear vector-valued function arising from some discretization of PDE given by $F = (F_1, F_2, \dots, F_n)^T$ with $F_i = F_i(x_1, x_2, \dots, x_n)^T$, and $x = (x_1, x_2, \dots, x_n)^T$. To begin with, let us introduce a right nonlinear preconditioned system [35]

$$W(y) \equiv F(G(y)) = 0, \quad (2)$$

where

$$x = G(y)$$

acts as a nonlinear preconditioner, and the Jacobian matrix of (2) takes the form

$$\frac{\partial W}{\partial y} = \frac{\partial F}{\partial G} \frac{\partial G}{\partial y}.$$

Assume that the current approximation, $y^{(k)}$, is available. Then, INB used for solving $W(y) = 0$ suggests that the new approximation is obtained via

$$y^{(k+1)} = y^{(k)} + \alpha \Delta y^{(k)} \quad (3)$$

where $\Delta y^{(k)}$ is the solution of the following Jacobian system

$$\frac{\partial W(y^{(k)})}{\partial y} \Delta y^{(k)} = -W(y^{(k)}),$$

or

$$\frac{\partial F(x^{(k)})}{\partial G} \frac{\partial G(y^{(k)})}{\partial y} \Delta y = -F(G(y^{(k)})), \quad (4)$$

Let $\Delta x^{(k)} = \frac{\partial G(y^{(k)})}{\partial y} \Delta y^{(k)}$ and we apply G to both sides of (3) to obtain

$$\begin{aligned} G(y^{(k+1)}) &= G(y^{(k)} + \alpha \Delta y) \\ &\approx G(y^{(k)}) + \alpha \frac{\partial G(y^{(k)})}{\partial y} \Delta y^{(k)} \end{aligned}$$

Here, the first-order Taylor's expansion around $y^{(k)}$ is applied. Hence,

$$x^{(k+1)} = x^{(k)} + \alpha \Delta x^{(k)}, \quad (5)$$

where

$$\frac{\partial F(x^{(k)})}{\partial G} \Delta x^{(k)} = -F(x^{(k)}), \text{ with } x^{(k)} = G(y^{(k)}) \quad (6)$$

Note that we have two possible ways to solve (1) by using a right nonlinear preconditioned INB method. Either in the preconditioned solution space for the y -variable is as described by Steps (4) and (3) or in the solution space for the x -variable is as given by Steps (6) and (5). In general, these two approaches are not mathematically equivalent, unless using the linearization of G , since the operator G and the solution update (5) do not commute. From a practical viewpoint, the latter approach is more preferable than the first one, because the first formulation has the following potential drawbacks. The operator $G(y)$ is implicitly defined so that the Jacobian of $G(y)$ is hard to obtain. Moreover, designing an efficient preconditioner for the Jacobian system in the composite form in (4) is quite challenging. Hence, in this paper, we adopt the

second approach and confine our discussion to a right preconditioner $G(y)$ based on the nonlinear elimination algorithm. We first describe INB for (1) in conjunction with nonlinear elimination preconditioning for scalar PDE problems [20], and then generalize it to the multicomponent PDE problem in Section 4.

Let $S = \{1, 2, \dots, n\}$ be an index set and each index corresponds to an unknown component x_i and a nonlinear residual component, F_i . Supposedly, we can classify the nonlinear residual components, F_1, F_2, \dots, F_n , into two groups, namely the “good components” and “bad components”, respectively. Let k be the global Newton iteration number. Assume that $S_b^{(k)}$ (“b” for bad) is a subset of S with $m^{(k)}$ components and $S_g^{(k)}$ (“g” for good) with $(n - m^{(k)})$ components is its complement; that is

$$S = S_b^{(k)} \cup S_g^{(k)} \quad \text{and} \quad S_b^{(k)} \cap S_g^{(k)} = \emptyset \quad (7)$$

Usually $m^{(k)} \ll n$. For this partition, we define two subspaces

$$V_b^{(k)} = \{v | v = (v_1, \dots, v_n)^T \in \mathbb{R}^n, v_i = 0 \text{ if } i \notin S_b^{(k)}\}$$

and

$$V_g^{(k)} = \{v | v = (v_1, \dots, v_n)^T \in \mathbb{R}^n, v_i = 0 \text{ if } i \notin S_g^{(k)}\},$$

respectively, and the corresponding restriction operators, $R_b^{(k)}$ and $R_g^{(k)}$, which map vectors from \mathbb{R}^n to $V_b^{(k)}$ and $V_g^{(k)}$, respectively. Using the restriction operator $R_b^{(k)}$, we define a nonlinear function $F_{S_b^{(k)}} : \mathbb{R}^n \rightarrow V_b^{(k)}$ as

$$F_{S_b^{(k)}}(y) = R_b^{(k)}(F(y)).$$

For any given $y \in \mathbb{R}^n$, $T_b^{(k)}(y) : \mathbb{R}^n \rightarrow V_b^{(k)}$ is defined as the solution of the following subspace nonlinear system,

$$F_{S_b^{(k)}}(R_g^{(k)}y + T_b^{(k)}(y)) = 0. \quad (8)$$

Using the subspace mapping functions, we introduce a new global nonlinear function,

$$x = G^{(k)}(y) \equiv R_g^{(k)}y + T_b^{(k)}(y).$$

Note that for a given y , the evaluation of $G^{(k)}(y)$ is required to solve a nonlinear system corresponding to the subspace $V_b^{(k)}$ by using typically the classical INB algorithm. The superscript k indicates the adaptivity of the nonlinear subspace function changes as the global Newton iterates. Now INB in conjunction with an adaptive nonlinear elimination (ANE) preconditioning can be described as follows.

ALGORITHM 1. Inexact Newton algorithm with backtracking technique-Adaptive nonlinear elimination preconditioning (INB-ANE).

Given an initial guess $x^{(0)}$ and set $k = 0$.

While $(\|F(x^{(k)})\| > \varepsilon^r \|F(x^{(0)})\|)$ and $(\|F(x^{(k)})\| > \varepsilon^a)$ do

Set $y^{(k)} = x^{(k)}$

(Application of ANE phase):

If $(\|F(x^{(k)})\| > \varepsilon_{switch})$ then

- Compute $x^{(k)} = G(y^{(k)})$ by solving (8) with INB.

else

- Set $x^{(k)} = y^{(k)}$

end if

(Global update phase):

- Inexactly solve the Jacobian system

$$J(x^{(k)})\Delta x^{(k)} = -F(x^{(k)}). \quad (9)$$

by some Krylov subspace method [29], e.g. GMRES or BiCGstab in conjunction with a preconditioner.

- Update $x^{(k+1)} = x^{(k)} + \lambda^{(k)} \Delta x^{(k)}$, where $\lambda^{(k)} \in (0, 1]$ is determined to satisfy

$$\|F(x^{(k)} + \lambda^{(k)} \Delta x^{(k)})\| \leq (1 - \alpha \lambda^{(k)}) \|F(x^{(k)})\|. \quad (10)$$

- Set $k = k + 1$.

End While

Remark 1. To employ the ANE algorithm as a nonlinear preconditioner, the user needs to provide a routine on his or her own to determine the partition of S in (7). An effective identification of the bad component to be eliminated contributes a critical success factor to the ANE preconditioned iterative method. However, designing such good strategy is often problem-dependent, and so far, no available theoretical analysis can be used for the design guideline. Generally speaking, the partition can be determined in two different ways, that is, in either static or dynamic fashion. For the former class, the partitioning is obtained beforehand based on the pre-knowledge of the problem to solve. such as when the nonlinearity of one field variable is stronger than the others in the multi-component PDE system. The index set corresponding to such field variable can be classified as bad components. One the other hand, the partition can be adaptive dynamically during the Newton iterations, see [20] for a successful example using the global intermediate solution to update the partition.

Remark 2. The parameter ϵ_{switch} determines the activation of ANE phase. When the residual norm, $\|F(x)\|$, is less than the pre-selected value of ϵ_{switch} , which implies that the intermediate numerical solution is close to the desired one, the nonlinear elimination step may be turned off. Then, the INB-ANE algorithm is reduced to be as the classical INB algorithm. In this situation, the local quadratic convergence property of the Newton method can often be retained and the overhead of the entire algorithm is reduced because ANE phase is kept to be minimal.

Remark 3. For left nonlinear preconditioned Newton-type algorithms, such as ASPIN, linear preconditioning in conjunction with Krylov subspace methods for the global Jacobian system is built-in by design [4]. The nonlinear additive Schwarz preconditioner automatically produces a better conditioned Jacobian than the one for the original nonlinear system. On the other hand, right nonlinear preconditioner provides flexibility for choosing the linear Jacobian solvers. A linear preconditioner designed for the Jacobian system of the original nonlinear problem can be applied. Commonly used preconditioners include the domain decomposition [31, 33], multigrid [29, 34], and block-type preconditioners [2]. On the other hand, the Jacobian system for the nonlinear subspace system may also need to be preconditioned, although in general, the subspace Jacobian system is better conditioned than the global Jacobian system.

3. Highly local nonlinear fluid flows and convective heat transfer problems

Let Ω be a bounded computational domain in \mathbb{R}^2 . We consider the incompressible fluid flow and convective heat transfer problems, which are modeled by the Navier-Stokes equations in the velocity-vorticity form [14] and the energy equation as follows.

$$\begin{cases} -\Delta u - \frac{\partial \omega}{\partial y} & = 0 & \text{in } \Omega, \\ -\Delta v + \frac{\partial \omega}{\partial x} & = 0 & \text{in } \Omega, \\ -\frac{1}{Re} \Delta \omega + u \frac{\partial \omega}{\partial x} + v \frac{\partial \omega}{\partial y} - \frac{Gr}{Re^2} \frac{\partial T}{\partial x} & = 0 & \text{in } \Omega, \\ -\frac{1}{RePr} \Delta T + u \frac{\partial T}{\partial x} + v \frac{\partial T}{\partial y} & = 0 & \text{in } \Omega, \end{cases} \quad (11)$$

where (u, v) is the velocity field in the x - and y -directions, respectively,

$$\omega = -\frac{\partial u}{\partial y} + \frac{\partial v}{\partial x} \quad (12)$$

is the component of the vorticity normal to the xy -plane (representing the in-plane rotation of an infinitesimal fluid element), and T is the temperature. Three non-dimensional parameters in the system include the Reynolds number (Re), the Grashof number (Gr), and the Prandtl number (Pr). In fluid mechanics, the Reynolds number quantifies the relative importance of two sources of forces, the inertial force and the viscous force provided that the given flow conditions. Similarly, the Grashof number provides a piece of information how an effect of the buoyancy force acting on a fluid element is more important compared to that of the viscous force. Some proper boundary conditions for each variable are needed to close the system. In this paper, we confine our discussion on the fluid flows within a square cavity, Ω defined in the domain, $(0, 1) \times (0, 1)$ with the boundary Γ , where $\Gamma_1, \Gamma_2, \Gamma_3$ and Γ_4 are the disjoint portions of the boundary Γ of the domain Ω , $C_1 \cup C_2 \cup C_3 \cup C_4$ are its corners, as shown in Fig. 1.

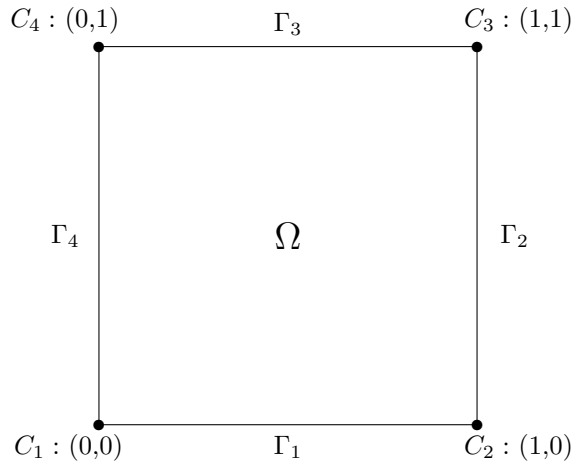


Figure 1: The computational domain $\Omega = (0, 1) \times (0, 1)$.

Two kinds of convective mechanisms for heat transfers are considered: forced convection and mixed convection cases. The first test case is the lid-driven cavity problem [14, 15]. The flow is assumed to be isothermal, hence the last term in the third equation of (11) involved the Grashof number $Gr = g\beta(T_H - T_C)/L^3\nu$ vanishes and the energy equation does not need to be solved together with the Navier-Stokes equations. Here, g is the gravity, T_H and T_C are the temperatures at the hot and cold walls, L are the length of the cavity, and ν is the viscosity, respectively. The boundary condition settings for the lid-driven cavity problem are given by

$$\begin{cases} u & = 1 & \text{on } \Gamma_3 \cup C_3 \cup C_4, \\ u & = 0 & \text{on } \Gamma / (\Gamma_3 \cup C_3 \cup C_4), \\ v & = 0 & \text{on } \Gamma, \\ \omega + \frac{\partial u}{\partial y} - \frac{\partial v}{\partial x} & = 0 & \text{on } \Gamma. \end{cases}$$

The second test case is the mixed convection cavity problem [9], in which the forced and natural convections both present simultaneously. In the case, we solve both of the fluid flow and energy equations (11), with

the following boundary conditions,

$$\left\{ \begin{array}{ll} u & = 1 \quad \text{on } \Gamma_3 \cup C_3 \cup C_4, \\ u & = 0 \quad \text{on } \Gamma/(\Gamma_3 \cup C_3 \cup C_4), \\ v & = 0 \quad \text{on } \Gamma, \\ \omega + \frac{\partial u}{\partial y} - \frac{\partial v}{\partial x} & = 0 \quad \text{on } \Gamma, \\ \frac{\partial T}{\partial y} & = 0 \quad \text{on } \Gamma/(\Gamma_2 \cup \Gamma_4), \\ T & = 1 \quad \text{on } \Gamma_2, \\ T & = 0 \quad \text{on } \Gamma_4. \end{array} \right.$$

Different from the lid-driven cavity problem, where the flows are mainly driven by the moving lid on the top wall, in the mixed convective cavity problem, the fluid flows are also driven by the buoyancy force due to temperature difference between the walls (The hot wall on the right ($T = 1$) and the cold wall on the left ($T = 0$)).

A standard central second-order finite difference scheme (both for the Laplacian operators and the first order partial derivatives) is used to discretize (11) in the domain Ω , together with the so-called efficient second order approximation for the vorticity equation (12) on the boundaries [28, 36] and other proper boundary conditions for each test case. Let Ω be covered with $n \times n$ mesh cells. Then each point $p_{i,j} = (x_i, y_j)$ is centered at the position $x_i = i \times h$ and $y_j = j \times h$ with $i, j = 1, \dots, n$, and $h = 1/(n - 1)$. In the study, we use the fully coupled ordering to build up the large sparse nonlinear algebraic system of equations (1), by which we mean that all four variables defined at the same mesh point $p_{i,j}$ are always together throughout the calculations. At each mesh point, we arrange the unknowns in the order of u_{ij} , v_{ij} , ω_{ij} , and T_{ij} , and then all mesh points numbered in the natural ordering. That is, the unknowns are ordered as

$$x = (u_{11}, v_{11}, \omega_{11}, T_{11}, u_{21}, v_{21}, \omega_{21}, T_{21}, \dots, u_{nn}, v_{nn}, \omega_{nn}, T_{nn})^T \quad (13)$$

and the corresponding functions are in the order of

$$F(x) = (F_{11}^{(u)}, F_{11}^{(v)}, F_{11}^{(\omega)}, F_{11}^{(T)}, F_{21}^{(u)}, F_{21}^{(v)}, F_{21}^{(\omega)}, F_{21}^{(T)}, \dots, F_{nn}^{(u)}, F_{nn}^{(v)}, F_{nn}^{(\omega)}, F_{nn}^{(T)})^T. \quad (14)$$

We would like to point out that the computational fluid dynamics literature often suggests that an upwinding technique should be employed for the gradient operator in the convective-dominated convection-diffusion type of equation to prevent the numerical solution from unphysical oscillations. To the best of the authors' knowledge, no similar result is available in the literature by using such simple numerical scheme as used here. Hence, we performed carefully the mesh independent test to validate our computer flow code. Since we focus on the development of the robust and efficient solution algorithm itself not on that of the numerical scheme, indeed, a more sophisticated numerical scheme can be used. Fig. 3 illustrates a set of the plots for the lid-driven cavity problem with $Re = 10^3$, 5×10^3 , and 10^4 , including the streamlines, the vorticity contours, and the vertical velocity profiles along the section $y = 0.5$ with a series of uniformly refined meshes ranging from 128×128 to 512×512 . We find that the computed velocity profiles are stable and converge as the mesh is refined and they are consistent with published benchmark solutions in, e.g., [14, 15]. Moreover, our streamline patterns in Fig. 3 match well when compared with the streamlines in the earlier study [17] by using the Navier-Stokes equations in the velocity-pressure formulation.

For the mixed convection problem, we fix both of the Prandtl number $Pr = 1$ and the Richardson number $Ri = Gr/Re^2 = 0.2$, then varies different values of the Reynolds number from 500 to 1500. Fig. 3 shows a series of solution plots, including the streamlines, the temperature contours as well as the vertical velocity profile along $x = 0.5$ with different meshes from 128×128 to 512×512 . From the right panel of the figure, we can see that the mesh independent velocity profile results are observed. Moreover, for the case of $Re = 500$, a total of three eddies are found from the streamline plots, where two eddies near the bottom are generated due to the temperature difference on the walls and the major eddy is mainly driven by the moving top wall. For the case of higher Re , these two eddies merge into a single vertex; Furthermore, the new major vertex becomes larger and moves closer to the top wall.

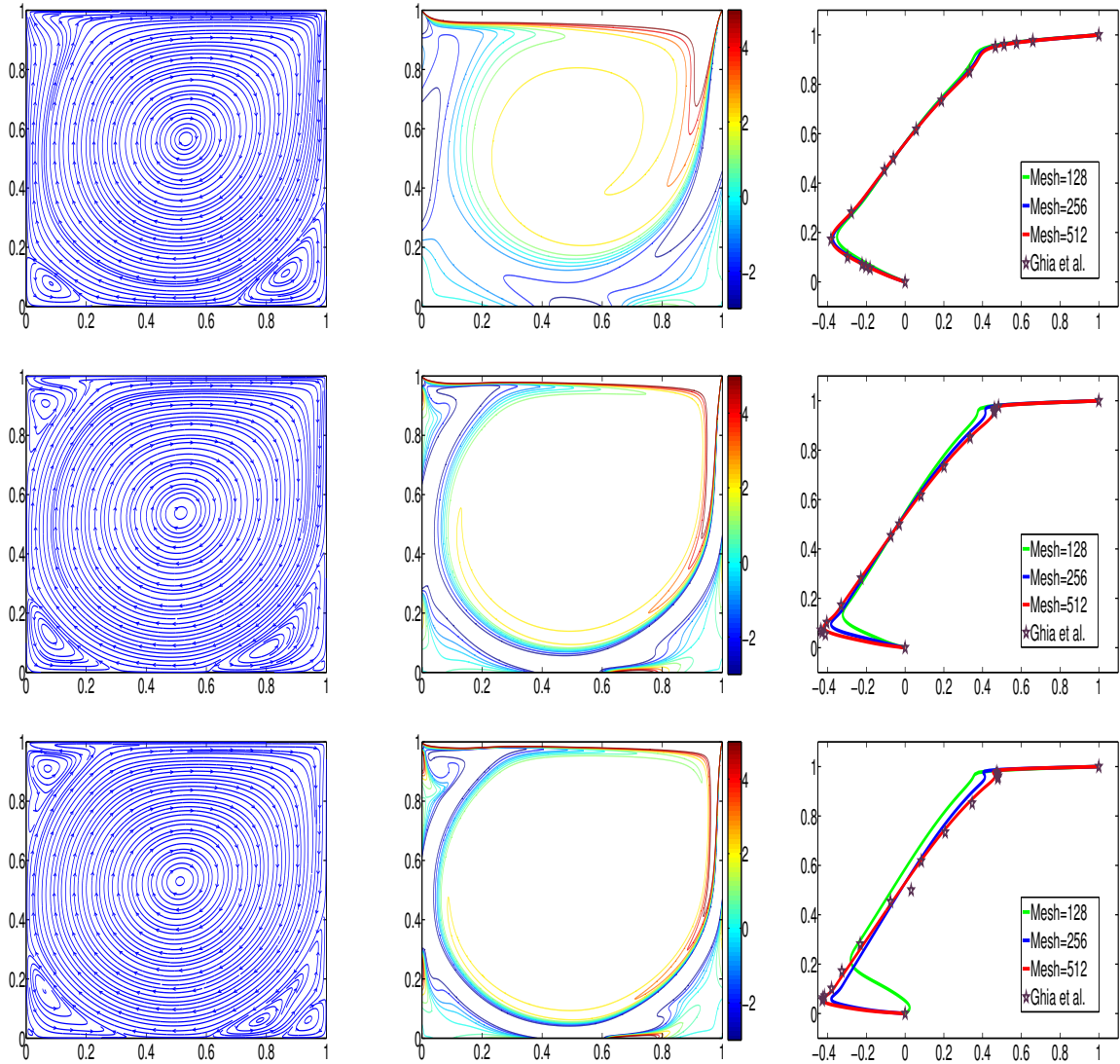


Figure 2: The lid-driven cavity problem. The streamlines (left column), the vorticity contours (middle column), and the u -component velocity profile curves on the along $x = 0.5$ for different mesh sizes (right column). $Re = 10^3$ (first row) $Re = 5 \times 10^3$ (second row) and $Re = 10^4$ (third row). The published results of Ghia et al. [15] are compared with the computed solutions.

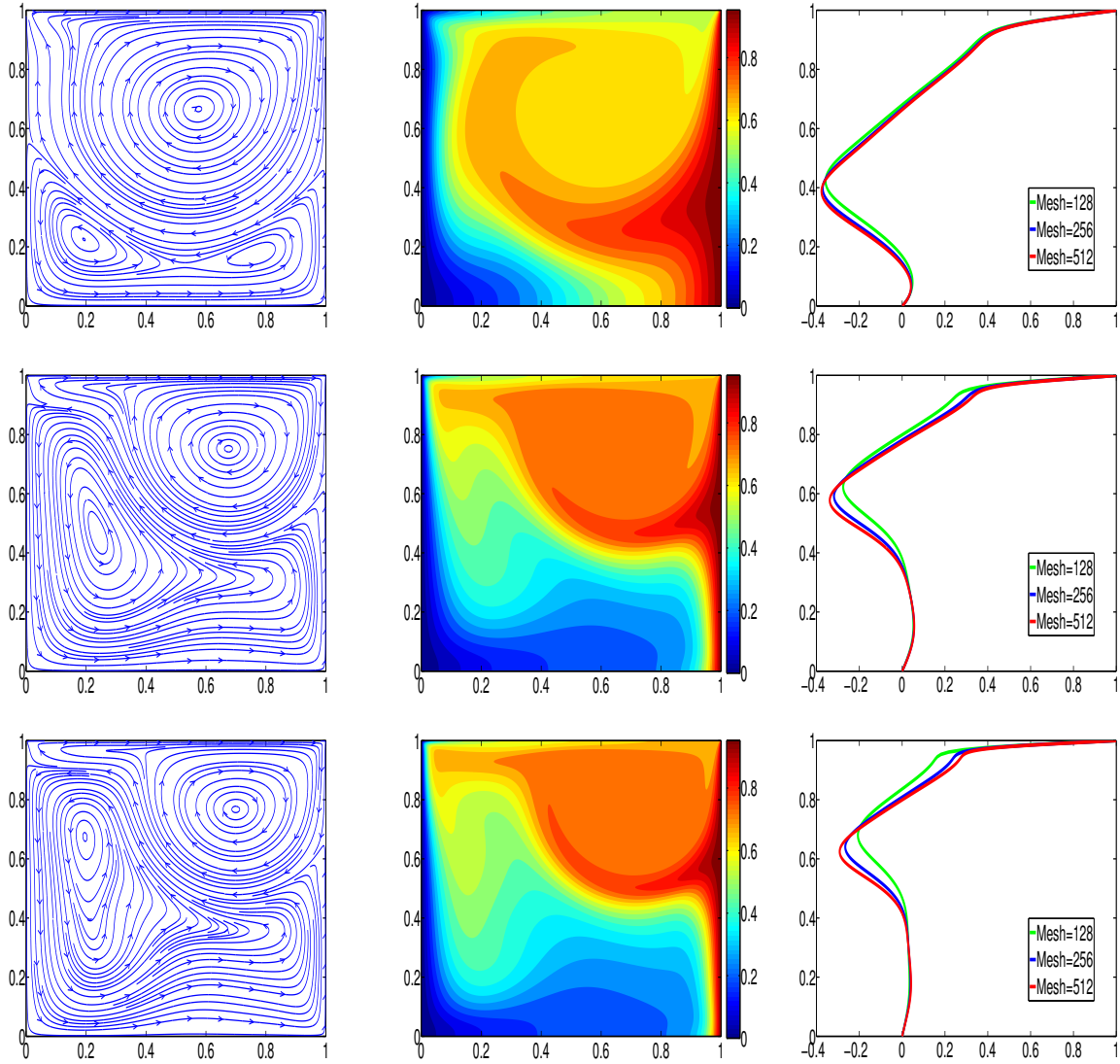


Figure 3: The mixed convection problem. The streamlines (first column), the temperature contours, (middle column), and the u -component velocity profiles on the along $x = 0.5$ for different mesh sizes (right column). $Re = 500$ (first row), $Re = 1000$ (second row), and $Re = 1500$ (third row).

Note that for both systems of large, sparse, nonlinear equations, the value of Re controls the degree of local nonlinearity. As Re increases, the classical INB algorithm is more difficult to converge to the desired solution. In Section 5, we will present detailed study for the robustness of INB with/without employing ANE preconditioner.

4. The ANE preconditioner for multi-component systems

For the sake of simplicity, we take the lid-driven cavity problem, a three-components system, as an example to illustrate how to construct the ANE preconditioner for the coupled system of PDEs. It can be extended to other nonlinear systems in a similar manner. We first introduce some notations. Let Ω^h be the collection of all mesh points in the computational domain and assume that each mesh point has 3-field variables. We partition Ω^h into two subsets such that $\Omega^h = \Omega_g^h \cup \Omega_b^h$, which are referred as “good” region and “bad” region, respectively. See Fig. 4 for an example of partitions of Ω^h with good and bad regions. Next, we define the subspace corresponding to the bad region, $V_b \subset \mathbb{R}^N$ as

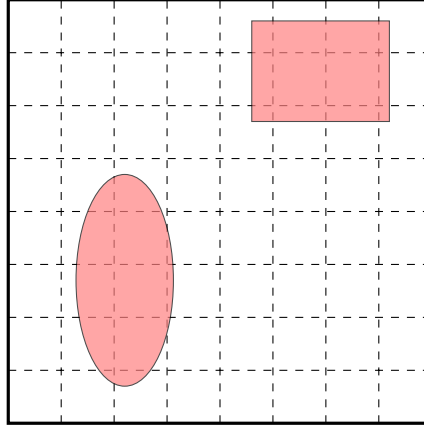


Figure 4: Partitions for the local iteration with good and bad components on a 9×9 mesh. The colored red subdomain means the collection of bad components in Ω_b^h and the uncolored subdomain means the collection of good components in Ω_g^h .

$$V_b = \{x | x = (x_{11}, \dots, x_{ij}, \dots, x_{nn})^T \in \mathbb{R}^N, x_{ij} = 0, \text{ if } p_{ij} \notin \Omega_g^h\}, \quad (15)$$

where $x_{ij} = (u_{ij}, v_{ij}, \omega_{ij})^T$. Similarly, we define the subspace corresponding to the good region.

$$V_g = \{x | x = (x_{11}, \dots, x_{ij}, \dots, x_{nn})^T \in \mathbb{R}^N, x_{ij} = 0, \text{ if } p_{ij} \notin \Omega_b^h\}, \quad (16)$$

In addition, the subspace V_g is further decomposed into V_g^w and $V_g^{w^c}$. For each subspace, we define the associated restriction and interpolation operators, that transfer the data on the whole domain to a subspace vice versa, including R_b , (I_b) , R_g^ω , (I_g^ω) , for the bad region and the vorticity components defined in the good region, respectively. For any given $y \in \mathbb{R}^N$, we define $M^b(y) : \mathbb{R}^N \rightarrow V_b$ and $M_\omega^b(y) : \mathbb{R}^N \rightarrow V_g^\omega$ as the solution of the following coupled nonlinear and linearized subspace systems,

$$\begin{cases} F_{V_b}(y + I_b M^b(y)) = 0 \\ L_{V_g^\omega}(y + I_g^\omega M_\omega^b(y)) = 0, \end{cases} \quad (17)$$

where $F_{V_b}(y) = R_b F(y)$ and $L_{V_g^\omega}(y)$ is the linearization of $R_g^\omega F(y)$ by assuming that u and v are known. In particular, for the lid-driven cavity problem, the coupled nonlinear system can be written explicitly as

$$\begin{cases} -\Delta_h u_{i,j} - \delta_y^0 \omega_{i,j} & = 0 \text{ in } \Omega_b^h \\ -\Delta_h v_{i,j} + \delta_x^0 \omega_{i,j} & = 0 \text{ in } \Omega_b^h \\ -\frac{1}{Re} \Delta_h \omega_{i,j} + u_{i,j} \delta_x^0 \omega_{i,j} + v_{i,j} \delta_y^0 \omega_{i,j} & = 0 \text{ in } \Omega_b^h, \\ -\frac{1}{Re} \Delta_h \omega_{i,j} + u_{i,j}^* \delta_x^0 \omega_{i,j} + v_{i,j}^* \delta_y^0 \omega_{i,j} & = 0 \text{ in } \Omega_g^h \\ u_{i,j} & = u_{i,j}^* \text{ on } \partial \bar{\Omega}_b^h \\ v_{i,j} & = v_{i,j}^* \text{ on } \partial \bar{\Omega}_b^h \end{cases}$$

where $\Delta_h \equiv \delta_x^2 + \delta_y^2$ is the standard five-point central difference operator defined on the point $p_{i,j}$ and δ_*^0 is the 2nd order central difference operator for the first partial derivatives in the x - or y -direction. Here $\bar{\Omega}_b^h$ is obtained by expanding one layer of the mesh points from Ω_b^h and $u_{i,j}^*$ and $v_{i,j}^*$ are the intermediate solution obtained from the previous Newton iteration. Using the subspace mapping function, we can introduce a new global function

$$x = G(y) \equiv R_g^\omega y + I_b M^b(y) + I_g^\omega M_g^\omega(y). \quad (18)$$

Hence, y is assumed to be a given known solution and the application of ANE for the multicomponent PDEs is done via the following two steps.

ALGORITHM 2 (Application of ANE $x = G(y)$).

(Determination of a partition of Ω^h).

Partition $\Omega^h = \Omega_g^h \cup \Omega_b^h$ based on the following rule,

$$\begin{cases} p_{i,j} \in \Omega_b^h, & \text{if any } |F_{ij}^{(*)}(x^k)| > \frac{\rho}{n} \|F(x^k)\|, * = u, v, \text{ or } \omega, \\ p_{i,j} \in \Omega_g^h, & \text{otherwise.} \end{cases}$$

Update the mesh transfer operators, R_b , I_b , R_g^ω , and I_g^ω .

(Subspace correction)

Solve the coupled subspace problems,

$$\begin{cases} F_{V_b}(y + I_b M^g(y)) = 0 \\ F_{V_g^\omega}(y + I_g^\omega M_g^\omega(y)) = 0 \end{cases}$$

for $M^b(y)$ and $M_g^\omega(x)$ by the inexact Newton method.

Compute $x = G(y) = R_g^\omega y + I_b M^b(y) + I_g^\omega M_g^\omega(y)$.

The elimination strategy proposed here is motivated by the observations from the intermediate classical Newton solution and associate point-wise residual plots as shown in Figures 5 and 6.

- **Highly local nonlinearity property.** Based on the knowledge of the incompressible fluid flow problem, we know that the resulting nonlinear problem becomes harder to solve when the strong singularity or boundary layer presents for the high Reynolds number cases. Moreover, from Fig. 5, we observe that the dominant part of the point-wise residual is the vorticity component ω of the global function at the upper right corner, and the orders of magnitude for the u - and v -components of the residual functions are 10^{-7} . In our approach, the criteria for determining the bad components to be eliminated is based on so-called hybrid physical-algebraic approach as follows: Let $\|F(x)\|$ be the nonlinear residual norm of the function vector and the absolute value of the component-wise residuals $|F_{ij}^{(*)}(x)|$ for the cases of $* = u, v, \text{ or } \omega$. A mesh point is classified as the point in the bad region if

$$|F_{ij}^{(*)}(x)| > \frac{\rho}{n_x} \|F(x)\| \quad (19)$$

where $\rho > 0$ is a pre-chosen constant and n is the number of mesh points in the x - or y -direction.

- Interfacial jump pollution reduction by including linearization of the vorticity equation defined in the good region.** Recall that, in [7], Cai and Li used a simple 1D nonlinear two-point boundary value problem to illustrate one potential computational problem of NE in practical applications: The intermediate numerical solution on or near the interface points between the good and bad regions may not be smooth. As a consequence, even tiny non-smoothness of some components can produce some large jumps in the residual function corresponding to those interface points because of some involved discrete derivative operators, such as gradient, divergence, etc. This phenomenon is also observed in our fluid flow problem, as shown in the left panel of Fig. 6. They also suggested that one should have some mechanism to reduce or remove such jumps to make the NE algorithm to be useful. Unfortunately, the *global update phase* in INB-ANE originally proposed in [20] cannot do such a good job for multicomponent problems as it did for scalar ones because each component interplays each other. The right panel of Fig.6 shows that these newly introduced jumps for the ω -component can not be smoothed out after the global update. It turns out that the interfacial jump pollution might cause a wrong judgment for choosing bad components properly, especially when the residual based criteria is employed. Those meshes corresponding to these new jumps are classified as the bad components mainly due to interfacial jump pollution. When the local nonlinear elimination phase cannot effectively remove highly local nonlinearity, the failure of global Newton iteration will happen. In the numerical result section, we will show that the inclusion of the auxiliary linearized ω subsystem in (17) is necessary for the convergence of the INB-ANE method.

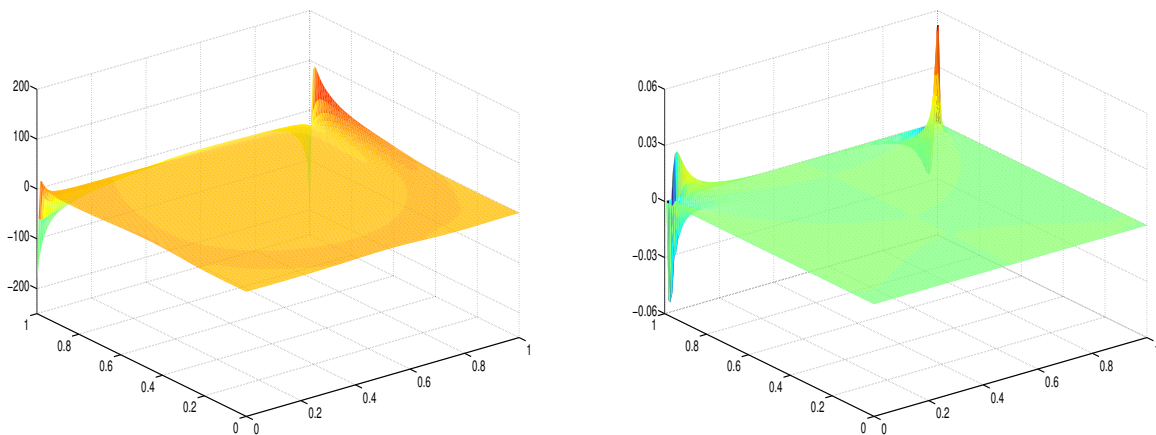


Figure 5: Lid-driven cavity problem. The left panel corresponds to the solution plot of the ω -component, and the right panel corresponds to the residual surface plot of the ω -component obtained after the first Newton's iteration. The calculation is carried out for $Re = 10^3$ on a 128×128 mesh. Note that the orders of magnitude for the residual function norm of u - and v -components are less than 10^{-7} after the first global Newton iteration.

Remark 4. The dimension of the nonlinear subspace system depends not only on the degree of the highly local nonlinearity but also the prescribed parameter ρ . The smaller the value of ρ is, the more the mesh points are classified as the bad points. In this case, the nonlinear subspace system may include too many unnecessary mesh points and the subsystem will become another highly local nonlinear system, which is difficult to be solved with INB.

Remark 5. After performing some slowness analysis, we understand that for the mixed convection problem, as Re , the dominate parts of the point-wise residual is the one corresponding to the subsystems for the vorticity and the temperature variables. Hence, we define the subspace system for this problem explicitly as follows.

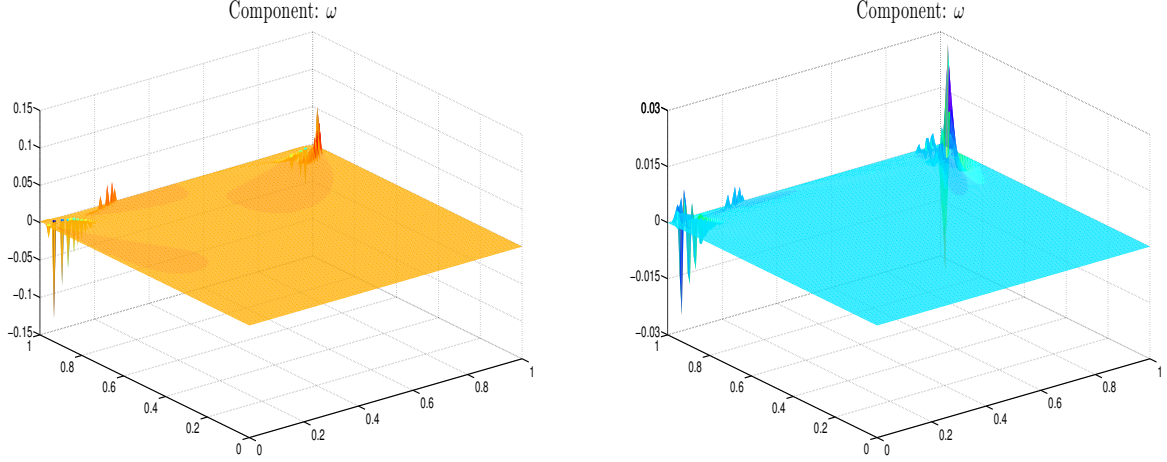


Figure 6: The lid-driven cavity problem. The plot of the residual surface for the u and ω -components obtained after the first subspace correction phase without the linearization part of (17). The left panel corresponds to the residual surface before the global update, and the right panel corresponds to the residual surface after the global update. Note that the distribution of the residual function for the v -component is similar to that for the u -component.

$$\left\{ \begin{array}{l} -\Delta_h u_{i,j} - \delta_y^0 \omega_{i,j} \\ -\Delta_h v_{i,j} + \delta_x^0 \omega_{i,j} \\ -\frac{1}{Re_1} \Delta_h \omega_{i,j} + u_{i,j} \delta_x^0 \omega_{i,j} + v_{i,j} \delta_y^0 \omega_{i,j} \\ -\frac{1}{RePr} \Delta_h T + u_{i,j} \delta_x^0 T + v_{i,j} \delta_y^0 T \\ -\frac{1}{Re_1} \Delta_h \omega_{i,j} + u_{i,j}^* \delta_x^0 \omega_{i,j} + v_{i,j}^* \delta_y^0 \omega_{i,j} - \frac{Gr}{Re^2} \delta_x^0 T \\ -\frac{1}{RePr} \Delta_h T + u_{i,j}^* \delta_x^0 T + v_{i,j}^* \delta_y^0 T \\ u_{i,j} \\ v_{i,j} \end{array} \right. \begin{array}{l} = 0 \text{ in } \Omega_b^h \\ = 0 \text{ in } \Omega_b^h \\ = 0 \text{ in } \Omega_b^h, \\ = 0 \text{ in } \Omega_b^h, \\ = 0 \text{ in } \Omega_g^h \\ = 0 \text{ in } \Omega_g^h \\ = u_{i,j}^* \text{ in } \partial \bar{\Omega}_b^h \\ = v_{i,j}^* \text{ in } \partial \bar{\Omega}_b^h \end{array}$$

5. Numerical results and discussions

In the section, we present some numerical results for two benchmark problems as described in Section 3, namely the lid-driven cavity problem and the mixed convection problem. The INB-ANE algorithm is implemented on top of the Portable, Extensible Toolkits for Scientific computation (PETSc, [1]) library. We carry out numerical experiments on a Dell supercomputer located at the University of Colorado Boulder, USA. In all the experiments, all Jacobian matrices are constructed approximately using a multi-colored finite difference method [10]. In INB-ANE, the nonlinear subspace problem (18) is solved by NKS until the stopping condition $\|G(x^{(k)})\| \leq 10^{-10}$ is satisfied. For the global problem, we continue the iteration until the convergence criterion given by

$$\|F(x^{(k)})\| \leq \max\{10^{-10}, 10^{-6}\|F(x^{(0)})\|\}.$$

The step length $\lambda^{(k)}$ in (10) is determined by a cubic line search technique [11, 13] with $\alpha = 10^{-4}$. In the INB-ANE and INB methods, a zero initial guess is used for the first Newton iteration for all test cases. Also, we use the restarted GMRES [29] method accelerated by an overlapping Schwarz preconditioning technique for solving the Jacobian problem inexactly (9),

$$\|F(x^{(k)}) + J^{(k)}(M^{(k)})^{-1}M^{(k)}\Delta s^{(k)}\| \leq \max\{\eta^r \|F(x^{(k)})\|, \eta^a\},$$

where $J^{(k)} = F'(x^{(k)})$ is the Jacobian matrix evaluated at $x^{(k)}$. The accuracy of the solution of GMRES is determined by a relative tolerance $\eta^r \in [0, 1)$ and an absolute tolerance $\eta^a \in [0, 1)$. $\eta^r = 10^{-6}$ and $\eta^a = 10^{-10}$ are selected. To define the Schwarz preconditioner $(M^{(k)})^{-1}$, we first begin by partitioning Ω

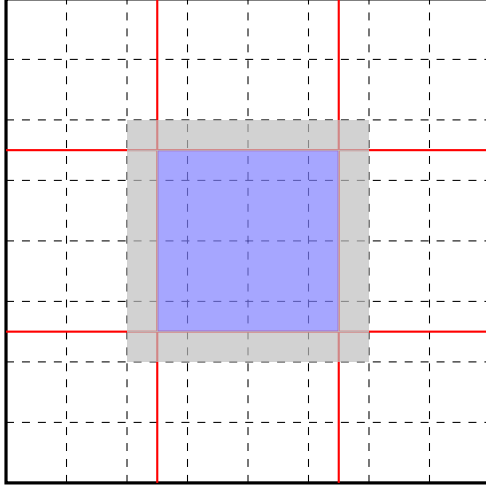


Figure 7: Partitions for the global iteration on a 9×9 mesh and 3×3 subdomains. The dashed lines indicate that the unit square domain is partitioned into 9×9 meshes, and the red lines indicate that the unit square domain is partitioned into 3×3 non overlapping subdomains.

into non-overlapping subdomains Ω_l , $l = 1, \dots, N_p$. Note that this partition is totally independent of the partition used for defining the subspace correction $G(y)$ in the Section 4. Then we expand each Ω_l to obtain Ω_l^δ , i.e., $\Omega_l \subset \Omega_l^\delta \subset \Omega$. The overlap $\delta > 0$ is defined as the distance between $\partial\Omega_l^\delta$ and $\partial\Omega_l$, in the interior of Ω . Let R_l^δ and R_l^0 be the restriction operator from Ω to its overlapping and non-overlapping subdomains, respectively. See Fig. 7 for an example of 3×3 overlapping partitions. Then the restricted additive Schwarz preconditioner [8, 31, 33] is defined as

$$(M^{(k)})^{-1} = \sum_{l=1}^{N_p} (R_l^0)^T (J_l^{(k)})^{-1} R_l^\delta$$

with $J_l^{(k)} = R_l^\delta J^{(k)} (R_l^\delta)^T$ and N_p is the number of subdomains, which is the same as the number of processors.

Throughout this section, in the tables, “Newton” denotes the number of inexact Newton iterations, “GMRES” denotes the average number of GMRES iterations per Newton iteration, and “Time” denotes the total computing time in seconds.

5.1. A comparison of INB and INB-ANE

We are especially interested in the cases in which INB fails to converge even when some globalization technique is used. In the left of Fig. 8, we compare both histories of the nonlinear residual norms of INB and INB-ANE for the lid-driven cavity problem with different $Re = 10^3, 5 \times 10^3$, and 10^4 on a 512×512 mesh. This figure indicates that the nonlinear system becomes harder to solve when the value of the Reynolds number increases. Also, the convergence behaviors of INB are quite similar, i.e., all nonlinear residual norms stagnate around 10^{-1} without any progress. We also noticed that for this particular mesh, INB starts to fail to converge for $Re = 750$, or above. On the other hand, the INB-ANE method converges nicely for a wider range of the Reynolds numbers. Also, as shown on the right of Fig. 8, we have similar results for the mixed convective flow problem. INB fails to converge at $Re=340$ or above and with help from the nonlinear

elimination preconditioner, INB-ANE can converge in less than 18 iterations for all test cases. Note that the INB-ANE results here are obtained after parametric tuning. The performance of the INB-ANE algorithm depends on several parameters involved such as the switch parameter, ϵ_{switch} and ρ . A detailed parametric study of these factors is presented in the next subsection.

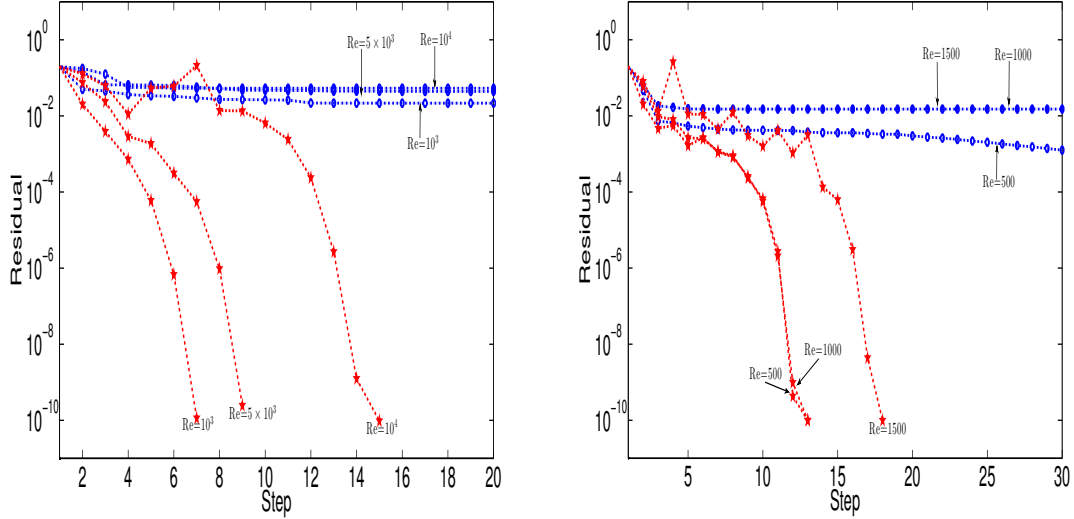


Figure 8: Histories of the nonlinear residual norms: Lid-driven cavity problem (left) for different Reynolds numbers, $Re = 10^3, 5 \times 10^3$, and 10^4 . Mixed convection problem (right) for different Reynolds numbers $Re = 500, 1000$, and 1500 . A 512×512 mesh is used. The symbol “ \star ” denotes INB-ANE and “ o ” denotes INB.

The main purpose of the nonlinear elimination acting as a nonlinear preconditioner is to remove the highly local nonlinear components of the system before performing the outer nonlinear iteration. Hence, the effective identification of the bad components to be eliminated plays an important role in the success of the method. Figures 9 and 10 show the evolution of the distribution of the bad components for first three global Newton iterations and the corresponding residual ω -component for both test problems. In the figures, the bad components are labeled with the red dots in the computational domain. These two figures indicate that all bad components are located near two top corners of the cavity, where the singularity or discontinuity of the solution is observed, especially for the ω -component. This series of plots suggests that our mechanism can be physically correct in identifying bad components.

5.2. Parametric study of the INB-ANE algorithm

In this subsection, we investigate how these two parameters, ρ and ϵ_{switch} , affect the overall performance of the INB-ANE algorithm. Using the lid-driven cavity problem as an example, we first study the effect of the switch parameter ϵ_{switch} on the convergence of the INB-ANE algorithm. We test the different values of ϵ_{switch} ranging from 10^{-6} to 10^{-1} and fix other parameters: $\rho = 1.5$, a 512×512 mesh, $Np = 64$, and $Re = 5,000$. Table 1 shows the number of Newton iterations for the global nonlinear problem and the nonlinear subspace problems as well as the average number of GMRES iterations per Newton for different values of ϵ_{switch} . From this table, we find that the number of global Newton iterations is insensitive to ϵ_{switch} as long as the preselected ϵ_{switch} is not too large, e.g., 10^{-1} for this case. If we turn off the ANE step too early, the bad components in the system may not be removed thoroughly and result in the divergence of the global iteration. On the other hand, when the mild value of ϵ_{switch} , say 10^{-2} , is set, one can save the computational cost for solving the nonlinear subspace problems, while maintaining the fast convergence of the global Newton method. In this case, we can save about 50% of the total time compared to the one obtained by the INB-ANE, where the ANE step is always turned on.

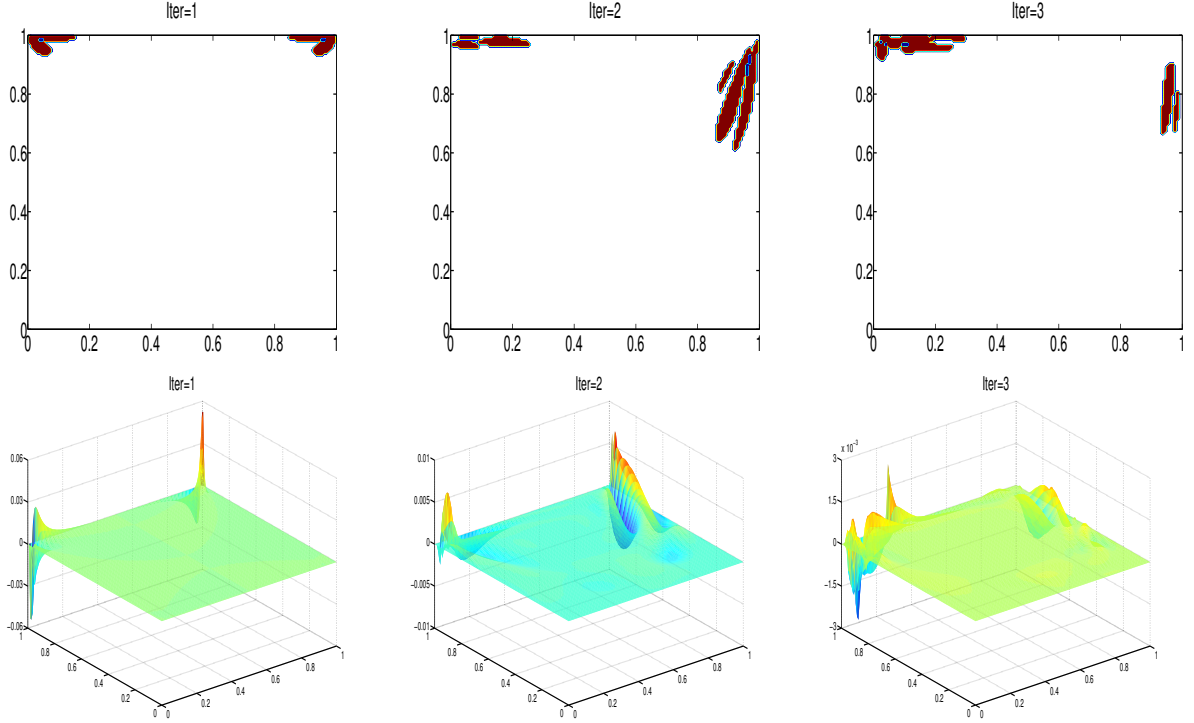


Figure 9: The lid-driven cavity problem. The evolution of distribution of the to-be-eliminated bad components (The first row) and the residual surface of the ω -component of the residual function (The second row) during the global Newton iterations. The problem is solved on a 128×128 mesh, $Re = 10^3$, $\epsilon_{switch} = 10^{-2}$ and $\rho = 3$. In this case, seven iterations are needed to reach convergence, and the orders of magnitude for the u - and v -components of the residual functions are 10^{-7} after the first global Newton iteration.

Table 1: The effect of switch parameter ϵ_{switch} for the lid-driven cavity problem. A 512×512 mesh, $N_p = 64$, $Re = 5 \times 10^3$ are considered. The “--” means divergence of the global iteration. In the global iteration, “Newton” denotes the overall number of inexact global Newton iterations; in the local iteration, “Newton” denotes the overall number of inexact subspace Newton iterations; and others defined in a similar way.

ϵ_{switch}	Newton	GMRES	Time	Newton	GMRES	Time	Total time
	Global iteration			Local iteration			
10^{-1}	--	--	--	--	--	--	--
10^{-2}	9	319.2	69.2	11	120.0	36.7	105.9
10^{-3}	10	281.8	68.6	21	115.3	52.3	120.9
10^{-4}	11	249.7	68.0	24	112.3	70.0	138.7
10^{-6}	11	251.2	68.6	26	109.8	78.9	147.5

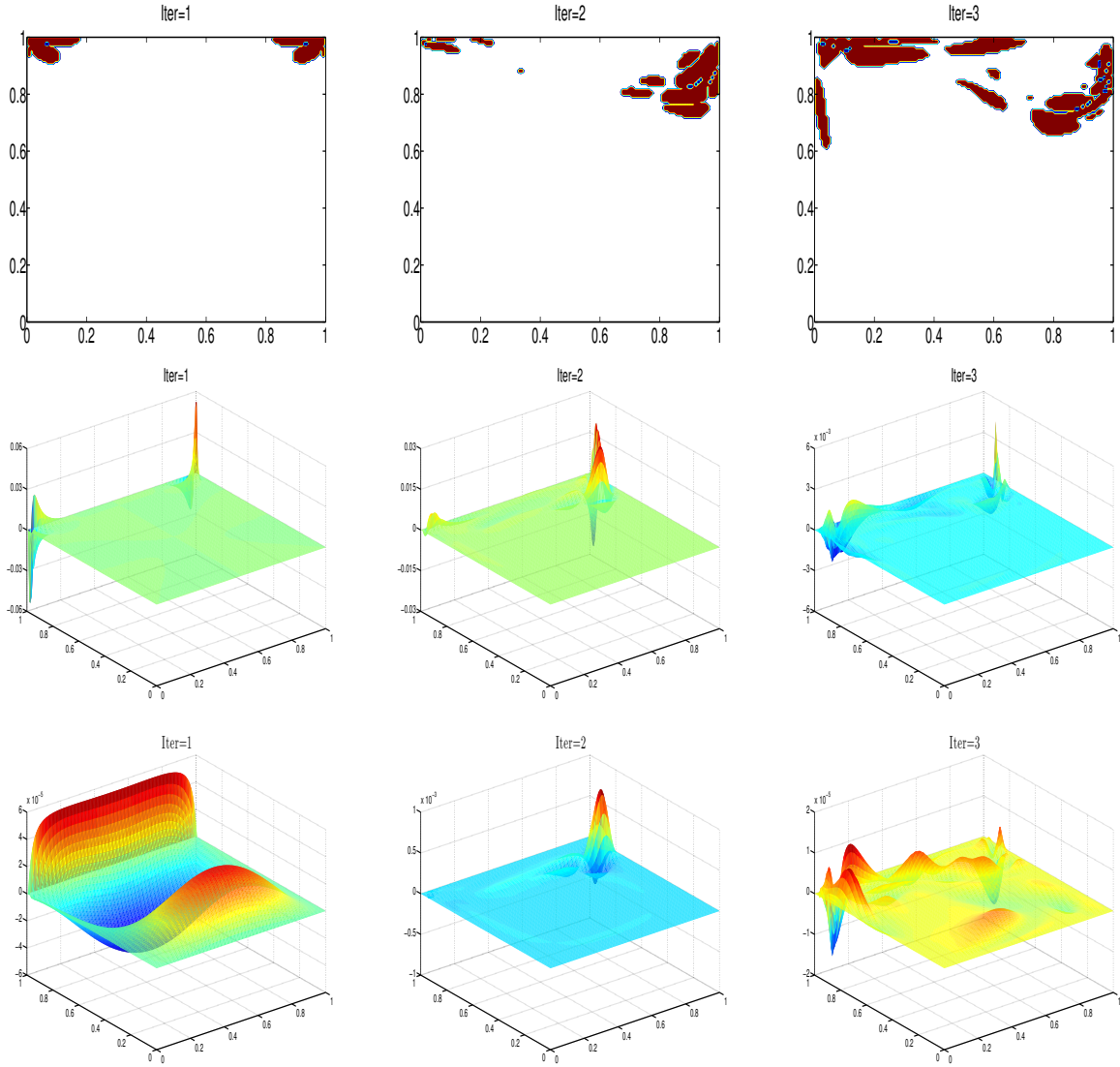


Figure 10: The mixed convection problem. The evolution of distribution of the to-be-eliminated bad components (The first row), the residual surface of the ω -component of the residual function (The second row), and the residual surface of the T component of the residual function (The third row) during the global Newton iterations. The problem is solved on a 128×128 mesh, $Re = 10^3$, $\epsilon_{switch} = 10^{-2}$ and $\rho = 3$. In this case, 13 iterations are needed to reach convergence, and the orders of magnitude for the u - and v -components of the residual functions are 10^{-7} after the first global Newton iteration.

Next, we study the impact of the value of ρ on the performance of INB-ANE and summarize the results with different Re for two test cases in Table 2. $N_p = 64$ is used on a 512×512 mesh. A fixed switch parameter ϵ_{switch} is set to 10^{-2} . From this table, we found that the number of global Newton iterations is less sensitive to the choice of ρ when the local nonlinearity is not strong for both cases. On the other hand, for the case with strong local nonlinearity, we need to choose a proper ρ more carefully. The optimal values of ρ can be found numerically. For the lid-driven cavity problem with $Re = 10^4$ and the mixed convective problem with $Re = 1500$, we have $\rho = 3.0$ and $\rho = 2.0$, respectively. Away from the optimal value, either too small or too large, the INB-ANE method may fail to converge. For the former case, as stated in Remark 6, we include too many unnecessary components so that subspace correction system becomes another nonlinearly unbalanced system. One possible solution is to introduce one additional nonlinear preconditioner for the subspace correction system. We refer to Ref. [19] for application of two-level nonlinear elimination preconditioners to one-dimensional quasi transonic problems.

5.3. Comparison to the field variable elimination strategy

For the purpose of comparison to our proposed algorithm, we considered another elimination strategy based on the field variable, for the case of the lid-driven cavity problem; that is, all the vorticity variables are eliminated. The subspace correction system is explicitly defined as follows:

$$-\frac{1}{Re} \Delta_h \omega_{i,j} + u_{i,j}^* \delta_x^0 \omega_{i,j} + v_{i,j}^* \delta_y^0 \omega_{i,j} = 0 \text{ in } \Omega^h, \quad (20)$$

where $u_{i,j}^*$ and $v_{i,j}^*$ are known. Note that Subproblem (20) is linear, and this system can be viewed as the Oseen-type linearization of (14). As a result, this type of the nonlinear preconditioner is reduced as the linear one. Then INB-ANE-field can be understood as the right linear subspace preconditioned Newton algorithm. Table 3 shows the results obtained with the field variable elimination strategy, labeled as INB-ANE-field and our proposed method for the lid-driven cavity problem with $Re = 5,000$ and $10,000$. For the case of a mild value of Reynolds or on the coarser mesh, the linear field variable elimination can improve the convergence of INB slightly, but it still fails for the case of the higher Reynolds number on finer mesh when the local nonlinearity becomes stronger. On the other hand, INB-ANE outperforms INB-ANE-field in terms of the robustness and efficiency. INB-ANE can not only converge nicely for a larger range of the Reynolds number but can also reduce the number of Newton iterations and the computing time significantly.

6. Concluding remarks

In this paper, we developed a nonlinear elimination preconditioned inexact Newton method for the multi-component PDE systems with highly local nonlinearity. The two key elements of the method are the valid identification of the to-be-eliminated components and the choice of subspace correction systems. In the method, we used the point-wise residual component of nonlinear systems as an indicator for selecting these to-be-eliminated components adaptively and built a subspace nonlinear system consisting of the components corresponding to the bad region and an auxiliary linearized subsystem to reduce the interfacial jump pollution. As numerical examples, we studied the performance of the new algorithm for solving the incompressible fluid flow and convective heat transfer problems at high Reynolds numbers. Our numerical results showed that we could restore the fast convergence of the Newton method by removing the strong localized nonlinearities with ANE. As a result, the global iteration counts depend on the Reynolds number mildly. Some possible future research works include an extension of the methods to some more general and more complicated problems, such as the system arising from an unstructured finite element method or multi-physics problems.

Acknowledgments

The first author was supported in part by the National Natural Science Foundation of China (11571100) and the state key laboratory program of LASG (20170062) and the second author was supported in part by the Ministry of Science and Technology, Taiwan, MOST-103-2115-M-008-007. The authors thank Prof. Xiao-Chuan Cai for useful discussion.

Table 2: The different choices of ρ . The lid-driven cavity problem and the mixed convection problem for different Reynolds numbers. $N_p = 64$ for the cases of a 512×512 mesh. The switch parameter $\epsilon_{switch} = 10^{-2}$. In the global iteration, “Newton” denotes the overall number of inexact global Newton iterations; in the local iteration, “Newton” denotes the overall number of inexact subspace Newton iterations; and others defined in a similar way.

Lid-driven cavity problem								
Re	ρ	Newton	GMRES	Time	Newton	GMRES	Time	Total time
		Global iteration			Local iteration			
10^3	0.1	8	155.1	30.2	8	70.6	14.9	45.1
	0.5	8	154.5	29.8	7	66.1	11.9	41.7
	1.0	7	157.0	26.2	6	75.0	10.6	36.8
	1.5	7	157.5	27.1	6	73.8	12.5	39.6
	2.0	7	158.4	28.2	6	72.3	11.5	39.7
5×10^3	1.0	9	310.0	68.0	12	114.0	33.7	101.7
	1.5	9	319.2	69.2	11	120.0	36.7	105.9
	2.0	9	307.7	67.5	12	116.9	33.1	100.6
	2.5	9	315.1	68.6	12	105.2	32.9	101.5
	3.0	9	307.3	67.2	13	104.4	29.9	97.1
10^4	2.5	--	--	--	--	--	--	--
	2.6	20	291.4	170.7	73	147.2	282.4	453.1
	3.0	15	272.2	118.2	36	149.5	138.0	256.2
	3.4	20	343.5	203.1	48	145.0	195.9	399.0
	3.5	--	--	--	--	--	--	--
Mixed convection problem								
500	0.1	14	167.5	91.5	35	106.0	139.1	230.6
	0.5	14	157.5	84.6	26	104.3	103.4	188.0
	1.0	13	171.1	81.4	22	104.8	86.3	167.7
	1.5	13	170.3	81.0	22	102.5	82.9	163.9
	2.0	13	171.4	83.4	22	100.2	79.6	163.0
	2.5	13	172.6	86.8	21	101.0	78.5	165.3
1000	0.1	13	193.0	94.5	28	112.3	112.6	207.1
	0.5	15	182.8	107.3	34	109.2	132.2	239.5
	1.5	18	196.2	142.3	39	105.6	172.2	314.5
	2.0	17	201.0	125.2	32	106.9	124.1	249.3
	2.5	17	204.1	134.6	32	106.0	123.0	257.6
1500	0.1	--	--	--	--	--	--	--
	0.5	33	268.6	332.7	97	156.0	550.9	873.6
	1.5	21	251.9	198.8	43	164.6	263.6	462.4
	2.0	18	252.1	170.1	35	130.9	169.0	339.1
	2.5	24	252.0	228.2	55	122.2	249.1	477.3

Table 3: A comparison of two possible elimination strategies for the lid-driven cavity problem. $N_p = 64$ for the cases of a 512×512 mesh and $N_p = 256$ for the cases of a 1024×1024 mesh. The “--” means divergence of the global iteration. In this table, “Newton” denotes the overall number of inexact global Newton iterations in global iteration, and others defined in a similar way.

Mesh	Re	Newton	GMRES	Time	Newton	GMRES	Time
		INB-ANE-field			INB-ANE		
512×512	5×10^3	12	244.4	80.9	9	307.3	67.2
	10^4	30	352.6	305.5	15	272.2	118.2
1024×1024	5×10^3	12	849.5	367.4	10	809.6	286.9
	10^4	--	--	--	17	1143.7	721.0

References

- [1] S. Balay, K. Buschelman, W.D. Gropp, D. Kaushik, M.G. Knepley, L. Curfman McInnes, B.F. Smith, and H. Zhang. PETSc Webpage, 2014. <http://www.mcs.anl.gov/petsc>.
- [2] M. Benzi, G.H. Golub, and J. Liesen. Numerical solution of saddle point problems. *Acta numerica*, 14:1–137, 2005.
- [3] X.-C. Cai, W.D. Gropp, D.E. Keyes, R.G. Melvin, and D.P. Young. Parallel Newton-Krylov-Schwarz algorithms for the transonic full potential equation. *SIAM J. Sci. Comput.*, 19:246–265, 1998.
- [4] X.-C. Cai and D.E. Keyes. Nonlinearly preconditioned inexact Newton algorithms. *SIAM J. Sci. Comput.*, 24:183–200, 2002.
- [5] X.-C. Cai, D.E. Keyes, and L. Marcinkowski. Nonlinear additive Schwarz preconditioners and applications in computational fluid dynamics. *Int. J. Numer. Meth. Fluids*, 40:1463–1470, 2002.
- [6] X.-C. Cai, D.E. Keyes, and D.P. Young. A nonlinear additive Schwarz preconditioned inexact Newton method for shocked duct flow. In *Domain Decomposition Methods in Science and Engineering*. CIMNE, 2002.
- [7] X.-C. Cai and X. Li. Inexact Newton methods with restricted additive Schwarz based nonlinear elimination for problems with high local nonlinearity. *SIAM J. Sci. Comput.*, 33:746–762, 2011.
- [8] X.-C. Cai and M. Sarkis. A restricted additive schwarz preconditioner for general sparse linear systems. *SIAM J. Sci. Comput.*, 21(2):792–797, 1999.
- [9] Y.A. Çengel and A.J. Ghajar. *Heat and Mass Transfer: Fundamentals & Applications*. McGraw-Hill, 2011.
- [10] Thomas F Coleman and Jorge J Moré. Estimation of sparse Jacobian matrices and graph coloring problems. *SIAM J. Numer. Anal.*, 20:187–209, 1983.
- [11] J.E. Dennis and R.B. Schnabel. *Numerical Methods for Unconstrained Optimization and Nonlinear Equations*. SIAM, Philadelphia, 1996.
- [12] V. Dolean, M. J. Gander, W. Kheriji, F. Kwok, and R. Massin. Nonlinear preconditioning: How to use a nonlinear Schwarz to precondition Newton’s method. *Preprint*, 2015.
- [13] S.C. Eisenstat and H.F. Walker. Globally convergent inexact Newton methods. *SIAM J. Optim.*, 4:393, 1994.
- [14] T. Fusegi and B. Farouk. Predictions of fluid flow and heat transfer problems by the vorticity-velocity formulation of the Navier-Stokes equations. *J. Comput. Phys.*, 65:227–243, 1986.
- [15] U. Ghia, K.N. Ghia, and C.T. Shin. High-Re solutions for incompressible flow using the Navier-Stokes equations and a multigrid method. *J. Comput. Phys.*, 48:387–411, 1982.
- [16] C. Groß and R. Krause. On the globalization of ASPIN employing trust-region control strategies—convergence analysis and numerical examples. *preprint*, 2011.
- [17] F.-N. Hwang and X.-C. Cai. A parallel nonlinear additive Schwarz preconditioned inexact Newton algorithm for incompressible Navier-Stokes equations. *J. Comput. Phys.*, 204:666–691, 2005.
- [18] F.-N. Hwang and X.-C. Cai. A class of parallel two-level nonlinear Schwarz preconditioned inexact Newton algorithms. *Comput. Meth. Appl. Mech. Eng.*, 196:1603–1611, 2007.
- [19] F.-N. Hwang, H.-L. Lin, and X.-C. Cai. Two-level nonlinear elimination-based preconditioners for inexact Newton methods with application in shocked duct flow calculation. *Electron. Trans. Numer. Anal.*, 37:239–251, 2010.
- [20] F.-N. Hwang, Y.-C. Su, and X.-C. Cai. A parallel adaptive nonlinear elimination preconditioned inexact Newton method for transonic full potential equation. *Comput. Fluids*, 110:96–107, 2015.
- [21] F.-N. Hwang, C.-Y. Wu, and X.-C. Cai. Numerical simulation of three-dimensional blood flows using domain decomposition method on parallel computer. *J. Chin. Soc. Mech. Eng.*, 31:199–208, 2010.
- [22] D.A. Knoll and W.J. Rider. A multigrid preconditioned Newton-Krylov method. *SIAM J. Sci. Comput.*, 21:691–710, 1999.
- [23] P.J. Lanzkron, D.J. Rose, and J.T. Wilkes. An analysis of approximate nonlinear elimination. *SIAM, J. Sci. Comput.*, 17:538–559, 1996.
- [24] L. Liu and D.E. Keyes. Field-split preconditioned inexact Newton algorithms. *SIAM J. Sci. Comput.*, 37:A1388–A1409, 2015.
- [25] L. Liu and D.E. Keyes. Convergence analysis for the multiplicative Schwarz preconditioned inexact Newton algorithm. *SIAM J. Numer. Anal.*, 54:3145–3166, 2016.
- [26] L. Liu, W. Zhang, and D.E. Keyes. Nonlinear multiplicative Schwarz preconditioning in natural convection cavity flow. In *Domain Decomposition Methods in Science and Engineering XXIII*, pages 227–235. Springer, 2017.
- [27] M. Pernice and M.D. Tocci. A multigrid-preconditioned Newton-Krylov method for the incompressible Navier-Stokes equations. *SIAM J. Sci. Comput.*, 23:398–418, 2001.
- [28] E.E. Prudencio, R. Byrd, and X.-C. Cai. Parallel full space SQP Lagrange-Newton-Krylov-Schwarz algorithms for PDE-constrained optimization problems. *SIAM J. Sci. Comput.*, 27:1305–1328, 2006.
- [29] Y. Saad. *Iterative methods for sparse linear systems*. SIAM, Philadelphia, 2003.
- [30] J.O. Skogestad, E. Keilegavlen, and J.M. Nordbotten. Domain decomposition strategies for nonlinear flow problems in porous media. *J. Comput. Phys.*, 234:439–451, 2013.
- [31] B.F. Smith, P.E. Bjørstad, and W. Gropp. *Domain Decomposition: Parallel Multilevel Methods for Elliptic Partial Differential Equations*. Cambridge University Press, 1996.
- [32] S. Sun, D.E. Keyes, and L. Liu. Fully implicit two-phase reservoir simulation with the additive schwarz preconditioned inexact Newton method. In *SPE Reservoir Characterization and Simulation Conference and Exhibition*. Society of Petroleum Engineers, 2013.
- [33] A. Toselli and O.B. Widlund. *Domain Decomposition Methods-Algorithms and Theory*. Springer-Verlag, Berlin, 2005.
- [34] U. Trottenberg, C.W. Oosterlee, and A. Schuller. *Multigrid*. Academic press, 2000.

- [35] H. Yang, F.-N. Hwang, and X.-C. Nonlinear preconditioning techniques for full-space Lagrange-Newton solution of PDE-constrained optimization problems. *SIAM J. Sci. Comput.*, 38:A2756–A2778, 2016.
- [36] H. Yang, E.E. Prudencio, and X.-C. Cai. Fully implicit Lagrange–Newton–Krylov–Schwarz algorithms for boundary control of unsteady incompressible flows. *Int. J. Numer. Meth, Engrg.*, 91:644–665, 2012.
- [37] H. Yang, C. Yang, and S. Sun. Active-set reduced-space methods with nonlinear elimination for two-phase flow problems in porous media. *SIAM J. Sci. Comput.*, 38:B593–B618, 2016.
- [38] D.P. Young, W.P. Huffman, R.G. Melvin, C.L. Hildes, and F. T. Johnson. Nonlinear elimination in aerodynamic analysis and design optimization. In L.T. Biegler, O. Ghattas, Heinkenschloss M., and B. van Bloemen Waanders, editors, *Large-Scale PDE-Constrained Optimization*, Lect. Notes in Comp. Sci., pages 17–44. Springer-Verlag, 2003.
- [39] M. Ziani. *Accélération de la convergence des méthodes de type Newton pour la résolution des systèmes non-linéaires*. PhD thesis, Université de Rennes 1, 2009.